AAS 20-528

RELATING COLLISION PROBABILITY AND MISS DISTANCE INDICATORS IN SPACECRAFT FORMATION COLLISION RISK ANALYSIS

Ulises E. Núñez Garzón[*] and E. Glenn Lightsey[†]

Active spacecraft formation flying collision avoidance schemes monitor collision risk through indicators such as miss distance and collision probability. This paper compares collision probability measures based on planar projections to their three-dimensional counterparts. In this analysis, it is found that the former overestimate the latter. Additionally, this work compares the consistency of risk assessments based on miss distance and collision probability. Certain statistics of relative position are well suited for collision risk assessments because their local minima and collision probability local maxima are anticorrelated, and vice versa. These results help connecting both types of indicators into a cohesive framework.

MOTIVATION

Spacecraft formation flying (SFF) is defined as a "set of more than one spacecraft whose dynamic states are coupled through a common control law".[1] Spacecraft formations are attractive from a space mission design perspective. In particular, SFF can enable missions with increased system robustness, as deterioration or failure of an agent in a spacecraft formation may only cause performance degradation in the mission, rather than causing the end of the mission.[2] Spacecraft formation missions may also have performance improvements over their mission lifetimes due to the ability to replace failed agents or add new ones. This adds a new layer to space mission architecture options beyond traditional, monolithic spacecraft missions.[3] Additionally, missions that implement SFF have an opportunity for enhanced system flexibility through improved "adaptability, scalability, evolvability, and maintainability".[4] Spacecraft formations can also enable high precision scientific missions by distributing a formation over regions larger than those spanned by large, monolithic spacecraft and by using sensor fusion.[5] Doing so has a plethora of applications, such as gravimetry,[6] weather forecasting and climate monitoring,[7] exoplanet detection,[8] gravitational wave detection,[9] and more.

The success of spacecraft formation missions is intrinsically linked with effective collision avoidance because formations are vulnerable to the threat of not only external collisions but also internal collisions. Since the threat of internal collisions is constant, methods of internal collision monitoring and avoidance must meet safety constraints while minimizing resource expenditure in order to extend mission lifetime.[2]

The existing literature in SFF collision avoidance (COLA) can be broadly divided into two categories: passive and active. Passive SFF COLA methods focus on passively safe formation designs. Using the terminology of Clohessy-Wiltshire (CW) relative orbital dynamics,[10,11] most of these passive SFF COLA methods account for the divergence of along-track uncertainty of the relative position of deputies with respect to chiefs by causing sufficient separation in the radial/cross-track plane.[12,13] These methodologies can be applied to spacecraft formation design, deployment, navigation and reconfiguration, without the need for COLA-dedicated maneuvers.[14–16] Other passive SFF COLA methods include separation in the "sky-plane" (i.e. in the along-track/cross-track plane),[17] energy matching,[18] and minimum range variation safety ellipses.[19]

[*]Graduate Research Assistant, Space Systems Design Lab, Guggenheim School of Aerospace Engineering, Georgia Institute of Technology, 620 Cherry St NW, Atlanta, GA 30332.

[†]Professor, Space Systems Design Lab, Guggenheim School of Aerospace Engineering, Georgia Institute of Technology, 620 Cherry St NW, Atlanta, GA 30332.

In active SFF COLA methods, collision risk is managed through predicting future motion of agents, determining whether the collision risk is acceptable, and if it is not, planning and executing COLA-dedicated maneuvers. Passive and active SFF COLA methods are not mutually exclusive, however, as active SFF COLA methods presuppose passively safe formation orbits as baselines. However, the distinction is made because it is possible to have formations that only implement SFF COLA passively, i.e. only with regular, autonomous station-keeping maneuvers every few orbits, as demonstrated by the TanDEM-X and PRISMA missions.[14,15] Active SFF COLA methods can be categorized by their collision risk indicators, i.e. by the measures used to conceptualize and mitigate risk. Once collision risk becomes unacceptable per such indicator, a correction signal is generally obtained by solving an optimal control problem, in which the risk is accounted for by setting appropriate constraints.

The first active SFF COLA method category comprises distance-based COLA methodologies, i.e. techniques that employ agent separation (e.g. inter-agent distance, or Cartesian components of relative position, etc.) to measure collision risk. Some miss distance-based COLA methods propose avoiding collision by setting appropriate inequality constraints directly in terms of the miss distance (or components of relative position).[20–28] Other miss distance-based COLA methods propose employing relative distance-based heuristics (e.g. artificial potential functions) to avoid collisions, applying the principles of swarm intelligence and distributed agent control theory.[29–34] A subset of distance-based active SFF COLA techniques account for state uncertainty directly in the formulation of the avoidance maneuvers by defining geometric collision regions (e.g. "covariance" contours, or reachable sets) that represent uncertainty envelopes.[27,28,33]

The second active SFF COLA method category comprises stochastic (or probabilistic) COLA methods, i.e. techniques whereby collision risk between pairs of agents is measured through the probability of the event that the relative position between agents is within a set that can be understood as a "collision region". This presupposes that the relative position is described by a probability distribution, which can be obtained as the outcome of relative state estimation.[35–37] Then, collision is avoided by designing a control signal that brings the probability of collision below an acceptable threshold. Some miss distance-based active SFF COLA methods do check collision probability,[25,34] while most stochastic active SFF COLA methods also check for miss distance.[36]

This work focuses on collision risk indicators for active SFF COLA. Specifically, the correlation relationship between miss distance and probability of collision is explored to understand whether these indicators provide consistent representations of collision risk. This contribution is beneficial for the following reasons:

1. In collision monitoring schemes where both collision risk indicators are used, the interpretation of risk as portrayed by one indicator may be enhanced by consideration of the other indicator.

2. In the more common case where only one collision risk indicator is used, this contribution may help understand the safety and performance tradeoffs of such a choice.

3. Under some circumstances, both collision risk waveforms may lead to the same qualitative conclusions, which would enable using them interchangeably. This would be true in the case that there was some statistic of relative position that both could be interpreted as miss distance and had the appropriate behavior when compared to probability of collision. That is, in this ideal case, at the same time, such a "miss distance"-like measure would locally indicate closest and furthest approach when probability of collision locally indicates highest and lowest collision risk, respectively, making the relationship consistent with intuition. This would be a valuable result for active SFF COLA methods that enforce miss distance constraints directly.

4. Additionally, for active SFF COLA methods that employ heuristics of miss distance, this contribution may help in the design of heuristics whose risk indication is consistent with what the probability of collision would indicate.

Overall, understanding the correlation relationship between miss distance and probability of collision is a step toward unifying both types of active SFF COLA methods into a single, coherent framework.

BACKGROUND

This section introduces some preliminaries. First, the notation used in this work is elaborated upon. Then, collision events are formally, topologically defined. Finally, Clohessy-Wiltshire (CW) relative orbital dynamics and geometry are discussed.

Notation

Vectors are underlined, while matrices and functions are not. Although boldface is reserved for multi-dimensional variables (i.e. vectors and matrices), sometimes boldfacing such variables may be avoided for clarity. Let $\underline{\mathbf{X}} \in \mathbb{R}^{n_{\underline{\mathbf{X}}}}$ and $\underline{\mathbf{R}} \in \mathbb{R}^{d_{\underline{\mathbf{R}}}}$ denote a dynamic state and position state, respectively. The dimensions of $\underline{\mathbf{X}}$ and $\underline{\mathbf{R}}$ are denoted by $n_{\underline{\mathbf{X}}}$ and $d_{\underline{\mathbf{R}}}$, resp. (Note: $d_{\underline{\mathbf{R}}} \in \{1, 2, 3\}$.) When used with the subscript i, $\underline{\mathbf{X}}_i$ and $\underline{\mathbf{R}}_i$ denote the dynamic state and position of agent i, resp. It is understood that $\underline{\mathbf{R}}_i$ specifically refers to the position of the center of mass of agent i. When used with a composite subscript such as "i-j", $\underline{\mathbf{X}}_{i,j}$ and $\underline{\mathbf{R}}_{i,j}$ denote the dynamic state and position of agent i and relative to agent j, resp., i.e. $\underline{\mathbf{X}}_{i,j} \doteq \underline{\mathbf{X}}_i - \underline{\mathbf{X}}_j$ and $\underline{\mathbf{R}}_{i,j} \doteq \underline{\mathbf{R}}_i - \underline{\mathbf{R}}_j$. When written in uppercase, $\underline{\mathbf{X}}$ and $\underline{\mathbf{R}}$ denote an uncertain dynamic state and uncertain position, resp., i.e. a dynamic state $\underline{\mathbf{X}}(t)$ and position $\underline{\mathbf{R}}(t)$ are random variables for any time t. Conversely, when written in lowercase, $\underline{\mathbf{x}}$ and $\underline{\mathbf{r}}$ denote specific, deterministic "instances" or values that $\underline{\mathbf{X}}$ and $\underline{\mathbf{R}}$ may take on, resp. When overlaid by a bar, $\bar{\underline{\mathbf{X}}}$ and $\bar{\underline{\mathbf{R}}}$ denote the expected (or "mean") values of $\underline{\mathbf{X}}$ and $\underline{\mathbf{R}}$, resp., i.e. $\bar{\underline{\mathbf{X}}} \doteq \mathbb{E}[\underline{\mathbf{X}}]$ and $\bar{\underline{\mathbf{R}}} \doteq \mathbb{E}[\underline{\mathbf{R}}]$.

When inside a square bracket and with a subscript outside of such bracket, $[\underline{\mathbf{R}}]_F \in \mathbb{R}^{d_{\underline{\mathbf{R}}}}$ denotes that $\underline{\mathbf{R}} \in \mathbb{R}^{d_{\underline{\mathbf{R}}}}$ is expressed in the coordinates of a reference frame F; similarly, $[a]_F \in \mathbb{R}$ denotes the a^{th} component of $\underline{\mathbf{R}}$ in the F-frame ($a \in \{x, y, z\}$). When $\underline{\mathbf{R}} \in \mathbb{R}^3$ can be expressed in the coordinates of a W-frame as $[\underline{\mathbf{R}}]_W^T = \left[[x]_W, [y]_W, [z]_W\right]$, and when overlaid by a tilde symbol, $[\widetilde{\underline{\mathbf{R}}}]_{\widetilde{W}} \in \mathbb{R}^2$ denotes the projection of $\underline{\mathbf{R}}$ onto the $\widetilde{W}$-projection plane (or simply $\widetilde{W}$), where $\widetilde{W}$ denotes the $[x]_W$-$[z]_W$ plane frame.

Definition of a collision event

A collision event (between two agents) occurs whenever their respective physical, nonempty "volumes" in $d_{\underline{\mathbf{R}}}$-dimensional space have a nonempty intersection. In other words, a collision event means that two agents may occupy portions of the same "volume" of space at the same time. The notion of a hard-body radius (or characteristic length) is used to simplify the definition of collision events, and consequently, the computation of the kinematic probability of collision (KPC). (Note: norm operations refer to the Euclidean norm.[38])

Definition 1 (n-ball[38])**.** The n-ball of radius r, centered at $\underline{x} \in \mathbb{R}^n$, denoted by $\mathbb{B}_r^n(\underline{x})$, is defined as the set

$$\mathbb{B}_r^n(\underline{x}) \doteq \{\underline{y} \in \mathbb{R}^n : \|\underline{x} - \underline{y}\| < r, r > 0\} \tag{1}$$

Note: when the dimension of elements in $\mathbb{B}_r^n(\underline{x})$ is implicit, it is referred to as $\mathbb{B}_r(\underline{x})$ for simplicity. ♢

Notation 2 (Characteristic length)**.** Let the "body of agent i", B_i, be defined as the set

$$B_i \doteq \left\{\underline{x} \in \mathbb{R}^{d_{\underline{\mathbf{R}}}} : \underline{x} \text{ is in the body of agent } i\right\} \tag{2}$$

Then, the i^{th} characteristic length, $l_i \in (0, \infty)$, is defined as

$$l_i \doteq \sup_{\underline{x} \in B_i} \|\underline{x} - \underline{\mathbf{r}}_i\| \tag{3}$$

Note: the body of agent i is circumscribed within $\mathbb{B}_{l_i}^{d_{\underline{\mathbf{R}}}}(\underline{\mathbf{r}}_i)$, i.e. $B_i \subseteq \mathbb{B}_{l_i}^{d_{\underline{\mathbf{R}}}}(\underline{\mathbf{r}}_i)$. ♢

Let i and j refer to two agents in proximity. Through the hard-body radius (HBR) simplification, illustrated in Figure 1, l_i represents a no-contact zone, i.e. agent j does not collide with any other agent j ($i \neq j$) if no point belonging to the body of agent j becomes closer to the i^{th} center of mass than a distance l_i. Thus, in order to avoid a collision with agent i, it is sufficient for agent j to be at least a distance l_i away from agent i, and vice versa. Using this intuition, the i-j collision event is now formally defined.

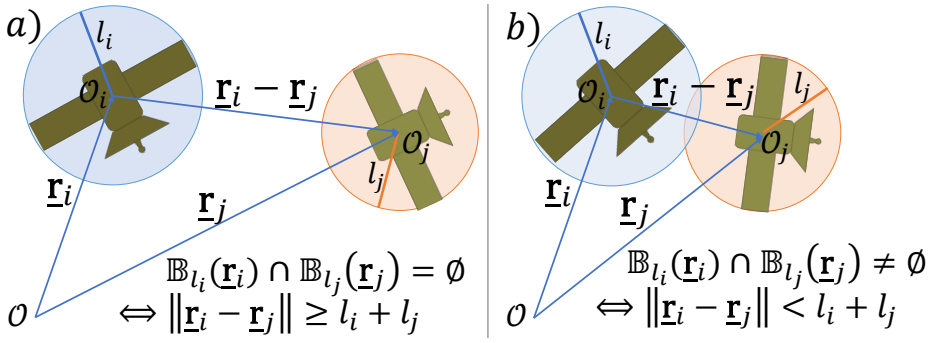

Figure 1: Agents i and j under the HBR simplification: a) no-collision condition, and b) collision condition. (Note: these circles represent $d_{\underline{\mathbf{R}}}$-balls that circumscribe the bodies of agents i and j, not position pdf's.)

Definition 3 (HBR simplification)**.** The body of agent i, B_i, satisfies $B_i = \mathbb{B}_{l_i}^{d_{\underline{\mathbf{R}}}}(\underline{\mathbf{r}}_i)$ by assumption. $\diamondsuit$

Definition 4 (Collision event)**.** Assume the HBR simplification holds (see Def. 3). Then, a collision event between agents i and j occurs when there is a nonempty intersection between the "volumes spanned" by agent i ($\mathbb{B}_{l_i}(\underline{\mathbf{r}}_i)$) and agent j ($\mathbb{B}_{l_j}(\underline{\mathbf{r}}_j)$), i.e. a collision occurs whenever

$$\mathbb{B}_{l_i}(\underline{\mathbf{r}}_i) \cap \mathbb{B}_{l_j}(\underline{\mathbf{r}}_j) \neq \emptyset \qquad \diamondsuit \tag{4}$$

In this subsection, collision events are topologically defined without any notion of the positions of colliding agents being random variables at the time of collision. Thus, if the relative positions of agents are known deterministically, the question of whether or not agents are colliding (in the sense that the conditions of Definition 4 are met, which may or may not imply not a physical collision) can be answered as either true or false, but not both. However, the primary aim of this work is to examine collision events when the relative position between agents is not deterministically known. In such cases, whether or not an object is colliding at any given time with another object is a question that can only be strictly answered in a probabilistic sense.

CW dynamics and geometry

Clohessy Wiltshire (CW) relative orbital dynamics refer to the dynamics of the motion of a "deputy" or "follower" agent with respect to a "chief" or "leader" agent. Under CW dynamics, it is assumed that the only force acting on each agent is the primary gravity from the central (planetary) mass in question, while higher order gravity terms and any other perturbations are neglected. Thus, the inertial trajectories of both agents are Keplerian orbits. CW dynamics also assume that the chief agent has a circular orbit, while the motion of the deputy agent about the chief spacecraft is assumed to be "small" compared to the chief orbit radius. The position of the deputy k about the chief c_0 ($[\underline{\mathbf{r}}_{k,c_0}]_H \in \mathbb{R}^3$, or simply $[\underline{\mathbf{r}}_k]_H$) is expressed in the coordinates of the Hill frame.[10] The CW relative dynamic state $[\underline{\mathbf{x}}_k]_H$ is completed by the relative position rate, i.e. $[\underline{\mathbf{x}}_k]_H^T = \left[[\underline{\mathbf{r}}_k]_H^T, [\dot{\underline{\mathbf{r}}}_k]_H^T\right]$. CW motion exhibits linear, time-invariant (LTI) dynamics; thus, the relative state $[\underline{\mathbf{x}}_k]_H(t)$ is related to its initial conditions through the c_0 state transition matrix (Φ_{c_0}) as $[\underline{\mathbf{x}}_k]_H(t) = \Phi_{c_0}(t, t_0)[\underline{\mathbf{x}}_k]_H(t_0)$, where

$$\Phi_{c_0}(t, t_0) = \begin{bmatrix} 4-3c & 0 & 0 & \frac{s}{n_{c_0}} & \frac{2}{n_{c_0}} - \frac{2c}{n_{c_0}} & 0 \\ -6n_{c_0}(t-t_0) + 6s & 1 & 0 & -\frac{2}{n_{c_0}} + \frac{2c}{n_{c_0}} & \frac{4s}{n_{c_0}} - 3(t-t_0) & 0 \\ 0 & 0 & c & 0 & 0 & \frac{s}{n_{c_0}} \\ 3n_{c_0}s & 0 & 0 & c & 2s & 0 \\ -6n_{c_0} + 6n_{c_0}c & 0 & 0 & -2s & -3+4c & 0 \\ 0 & 0 & -n_{c_0}s & 0 & 0 & c \end{bmatrix} \tag{5}$$

and where

$$c = \cos(n_{c_0}(t - t_0)) \tag{6}$$

$$s = \sin\left(n_{c_0}\left(t - t_0\right)\right) \tag{7}$$

Furthermore, if the CW trajectory of agent k about agent c_0 is closed, then the initial relative CW state $[\underline{\mathbf{x}}_k]_H(t_0)$ is constrained such that

$$[\dot{y}_k]_H(t_0) = -2n_{c_0}[x_k]_H(t_0) \tag{8}$$

Closed relative CW trajectories can be described in terms of the geometric parameters A_0, B_0, y_{off}, α_0 and β_0 as given by Equations 9, 10 and 11, in accordance with the notation of Schaub.[5] It should be noted that these are five, not six, geometric parameters, owing to the closed CW trajectory constraint, given by Eq. 8.

$$[x]_H(t) = A_0\cos\left(n(t - t_0) + \alpha_0\right) \tag{9}$$

$$[y]_H(t) = -2A_0\sin\left(n(t - t_0) + \alpha_0\right) + y_{\text{off}} \tag{10}$$

$$[z]_H(t) = B_0\cos\left(n(t - t_0) + \beta_0\right) \tag{11}$$

- A_0: amplitude of $[x]_H$ motion.
- y_{off}: steady-state offset of $[y]_H$ motion. Note: the amplitude of $[y]_H$ motion about y_{off} is $2A_0$.
- B_0: amplitude of $[z]_H$ motion.
- α_0: phase angle of $[x]_H$ motion. Note: the $[y]_H$ motion leads the $[x]_H$ motion by a phase difference of $\pi/2$, i.e. by 0.25 chief orbit periods, regardless of the value of α_0. Thus, the $[x]_H$-$[y]_H$ motion is always a 1:2 ellipse centered at $(0, y_{\text{off}})$.
- β_0: phase angle of $[z]_H$ motion.

The $\beta_0 - \alpha_0$ geometric parameter creates the greatest variability in the shape of closed CW trajectories. In particular, the following cases are noteworthy:

- $\mod(\beta_0 - \alpha_0, 2\pi) \in \{0, \pi\}$. Here, the $[x]_H$ and $[z]_H$ motions are in phase and are either correlated or anti-correlated, whereas the $[y]_H$ and $[z]_H$ motions are out of phase, creating a 2:(B_0/A_0) ellipse.
- $\mod(\beta_0 - \alpha_0, 2\pi) \in \{\pi/2, 3\pi/2\}$. Here, the $[x]_H$ and $[z]_H$ motions are in phase and are either correlated or anti-correlated, whereas the $[y]_H$ and $[z]_H$ motions are out of phase, creating a 1:(B_0/A_0) ellipse.
- $\mod(\beta_0 - \alpha_0, \pi/2) \neq 0$. Here, the $[z]_H$ motion is neither in phase nor out of phase with either the $[x]_H$ or $[y]_H$ motions, creating either correlated or anti-correlated ellipses in the $[x]_H$-$[z]_H$ and $[y]_H$-$[z]_H$ planes.

THEORY

Theoretical results on projection KPCs

In this work, the kinematic probability of collision (KPC), is defined as the probability that any two objects are in a "collision region" at any instant of time, based on the statistics of the relative position between the two objects at said time. Additionally, a distinction is made between the true KPC waveform and projection KPC waveforms. On one hand, the true KPC is computed over a three-dimensional (3D) collision region, based on the instantaneous, 3D probability density function (pdf) of the relative position. On the other hand, a projection KPC is computed over the two-dimensional (2D) collision region defined on a plane, based on the projection of the instantaneous, 3D relative position pdf onto said "projection plane". (In this work, a 2D collision region is defined as the projection of the 3D collision region onto an arbitrary projection plane.) In this paper, the relationship between true KPCs and projection KPCs is examined. This subsection motivates why developing these conceptual frameworks is beneficial to collision assessment activities.

There is extensive heritage for collision probability computation from the debris conjunction analysis and risk assessment (CARA) and debris COLA communities. In their practice, these communities often conceptualize the risk during a debris conjunction event to be equal to a projection KPC computed on the collision plane, which is normal to the relative velocity vector at the time of closest approach.[39,40] It is possible to conjecture that SFF collision risk can be adequately approximated by a projection KPC on a plane normal to the relative velocity vector. Additionally, in CW dynamics, radial/along-track motion is decoupled from cross-track motion. Thus, it is possible to conjecture that SFF collision risk can be approximated by a projection KPC on the radial/along-track plane.[33,35] Thus, before comparing KPC and miss distance waveforms, it is worthwhile to consider whether collision risk, in a kinematic sense, is adequately described by a projection KPC on any plane.

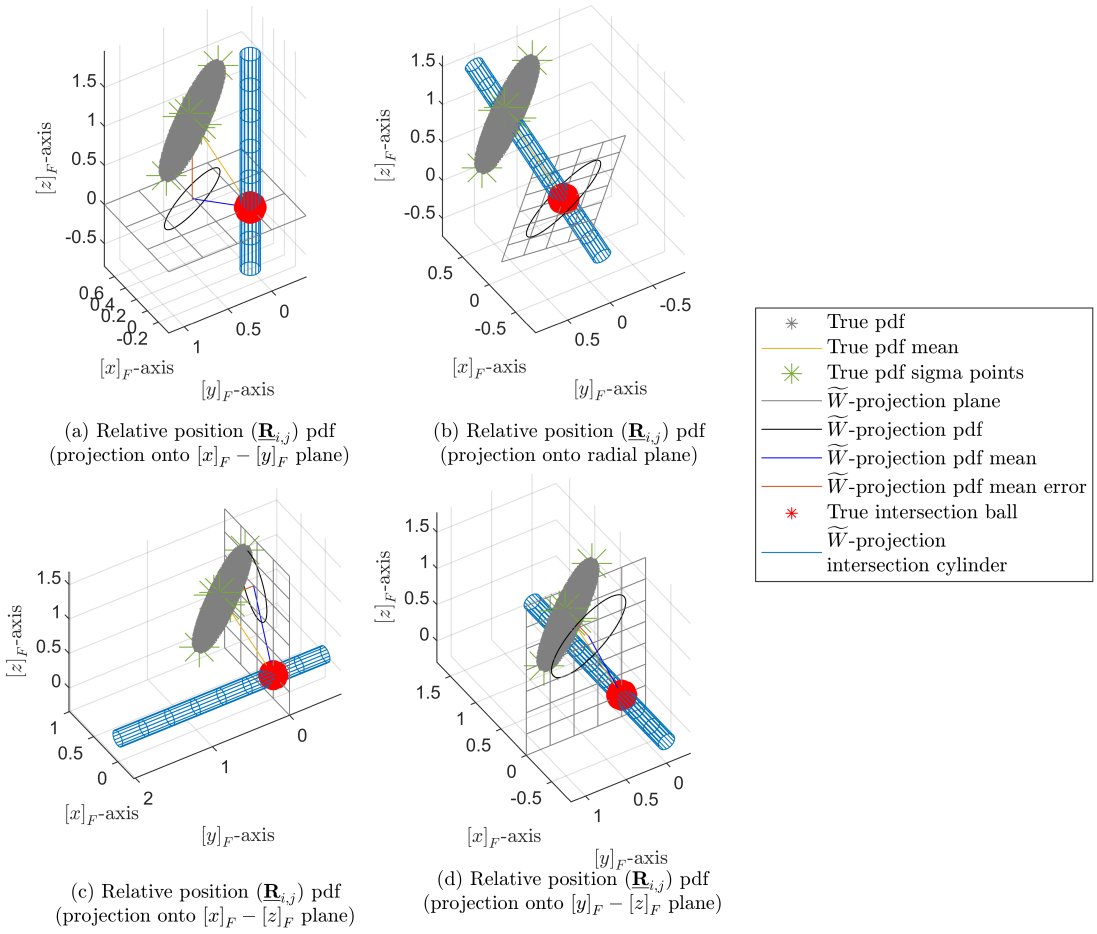

(a) Relative position ($\underline{\mathbf{R}}_{i,j}$) pdf (projection onto $[x]_F - [y]_F$ plane)

(b) Relative position ($\underline{\mathbf{R}}_{i,j}$) pdf (projection onto radial plane)

(c) Relative position ($\underline{\mathbf{R}}_{i,j}$) pdf (projection onto $[x]_F - [z]_F$ plane)

(d) Relative position ($\underline{\mathbf{R}}_{i,j}$) pdf (projection onto $[y]_F - [z]_F$ plane)

Figure 2: Difference between true KPC and $\widetilde{W}$-projection KPC measures for a three-dimensional relative position pdf (expressed in the coordinates of an arbitrary reference frame F), for several $\widetilde{W}$-projection planes: a) $[x]_F$-$[y]_F$, b) normal to expected relative position, c) $[x]_F$-$[z]_F$, and d) $[y]_F$-$[z]_F$.

Theorem 5 (Projection KPCs overestimate true KPCs)**.** Suppose the pdf of the relative position of agent i relative to agent j in $\mathbb{R}^3$ is known and continuous. Let W denote a Cartesian reference frame in $\mathbb{R}^3$. Let the $\widetilde{W}$-projection KPC refer to the KPC computed on the $\widetilde{W}$-projection plane (i.e. the $[x]_W$-$[z]_W$ plane). Then,

- Every $\widetilde{W}$-projection KPC is an overestimate of the true KPC.
- If $\text{support}\left(\text{pdf}_{\underline{\mathbf{R}}_{i,j}|t,t_0}\right) = \mathbb{R}^3$, then such $\widetilde{W}$-projection KPC is a strict overestimate of the true KPC.
- In particular, for the specific case of a nondegenerate, normally distributed relative position pdf, every $\widetilde{W}$-projection KPC is a strict overestimate of the true KPC. ♢

Proof. Omitted due to paper length limitation. □

Corollary 6. The $\widetilde{W}$-projection KPCs in the following $\widetilde{W}$-projection planes are overestimates of the true KPC:

- Every coordinate plane $\widetilde{W}$-projection KPC, i.e. for any arbitrary reference frame I, the $[x]_I$-$[y]_I$, $[x]_I$-$[z]_I$ and $[y]_I$-$[z]_I$ coordinate planes. Note: this particular result applies to any Hill frame H.
- Any plane whose normal vector is:
  - The expected value of the relative position pdf (also called a radial projection).
  - The expected value of the relative position rate pdf. ♢

Conceptually, true KPCs and projection KPCs are distinct, and this is shown through both theory and simulation. This concept is illustrated in Figure 2. Thus, if "KPCs" are to be used as criteria for triggering a COLA process, then it is evident that projection KPCs do not objectively satisfy the criteria for triggering such process, simply because projection KPCs are not in general equal to true KPCs. In particular, it is helpful to understand what distortions in conjunction assessments might be introduced when "greater than or equal" COLA trigger thresholds are implemented; that is, if planning and/or execution of COLA maneuvers occurs whenever the KPC goes above a fixed constant (which is a proxy for the maximum risk that can be tolerated).

Since projection KPCs are overestimates of true KPCs, using projection KPCs as COLA trigger criteria would lead to deeming collision risk greater than it truly is, which would be analogous to having probabilistic "false positives". On the other hand, a common constraint after collision avoidance maneuvers is that KPC be brought under a certain threshold (e.g. 1E-7) after a maneuver is conducted. Thus, using projection KPCs as post-maneuver constraint satisfaction criteria could lead to further correction efforts than warranted to "sufficiently" avoid collision risk. Accounting for scarce onboard resources, both observations show that, for the case at hand, using projection KPCs as collision safety criteria (i.e. either as COLA trigger criteria or as post-maneuver constraint satisfaction criteria) would result in a shorter mission lifetime than would be warranted with the chosen risk tolerance.

Validation of projection KPC theoretical results

In this work, general results are demonstrated about projection KPCs, one of which shows how projection KPCs always overestimate true KPCs regardless of projection plane choice, as illustrated in Figure 2, and as proven in Theorem 5. This theoretical finding is validated by Monte Carlo (MC) analysis. In this work, such MC simulation assumes CW relative orbital dynamics in Low Earth Orbit (LEO). Additionally, it is assumed that the statistics of the initial relative state of the deputy spacecraft have a nondegenerate, normal distribution. Numerical KPC waveforms (true and projected) are compared to the Monte Carlo-based KPC waveforms. Performing such a Monte Carlo simulation is challenging if the debris CARA community requirement that KPC values above 1E-7 are considered significant were to be adopted for SFF collision risk assessment.[41,42] An example of Monte Carlo sample relative position distribution is illustrated in Figure 3. Several relevant spacecraft proximity cases are studied: without cross-track motion, and with cross-track motion (in phase with radial motion, out of phase with radial motion, and more general cases).

Conjecture 7. Suppose that a Monte Carlo (MC) sample is made of a multivariate normal distribution. Suppose that events with a probability of p_{req} or lower can be ignored. Then, it is expected that significant events (i.e. events with probability greater than p_{req}) can be captured with a sample size N_{MC} that satisfies

$$N_{\text{MC}} \geq 30 \left\lceil \frac{1}{p_{\text{req}}} \right\rceil \qquad \diamondsuit \tag{12}$$

In this work, it is assumed that Conjecture 7 holds. Additionally, mirroring NASA CARA practice, it is assumed in this work that potential conjunction events with KPC less than $1E-7$ are insignificant. Thus, $p_{\text{req}} = 1E-7$, which implies that the MC sample size, N_{MC}, should satisfy $N_{\text{MC}} \geq 3.0E8$. Arbitrarily, N_{MC} is chosen as $N_{\text{MC}} = 3.2E8$.

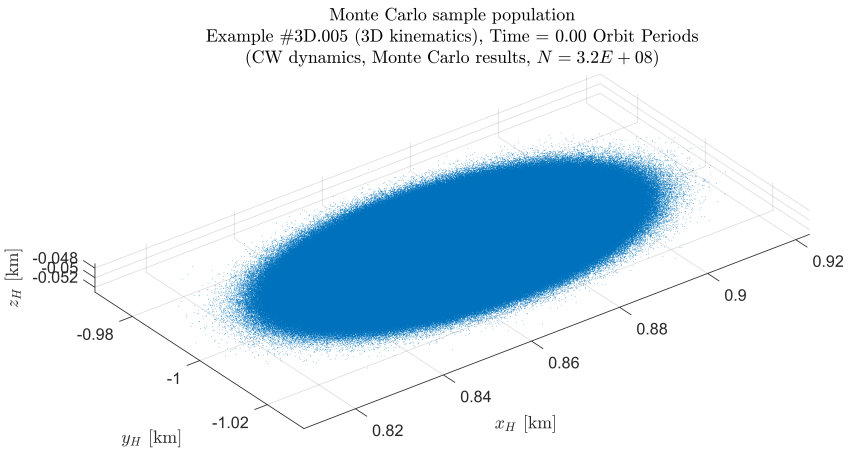

Figure 3: Monte Carlo sample prior relative position distribution (marginalization of sample relative state distribution).

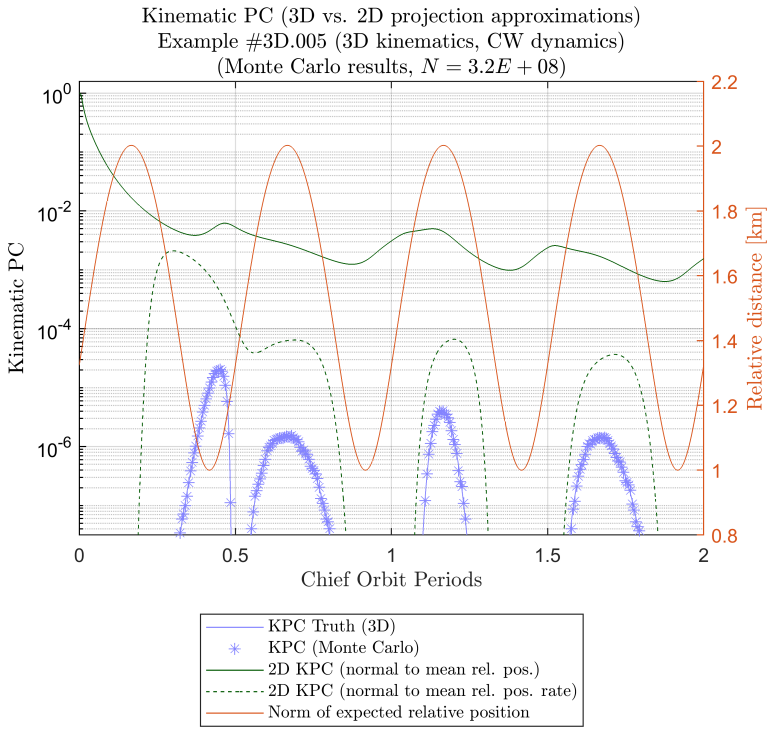

Figure 4: True KPC, projection KPCs and Monte Carlo KPC, with CW dynamics, closed orbit, normally distributed prior, Example 3D.005 (projection KPCs are normal to dynamics vectors).

Through the preceding Monte Carlo analysis, it is found that not only does the Monte Carlo KPC waveform converge to the true KPC waveform, but that the true KPC is significantly different from every projection KPC considered (i.e. those with projection planes normal to relative position and relative position rate, see Figure 4, and CW coordinate planes, see Figure 5). Even though there is some meaningful correlation between the true KPC waveform and some of the projection KPCs (i.e. for projection planes normal to relative position rate, and for the radial/along-track plane), this correlation is not consistent across cases, and the difference in magnitude could lead to different risk assessment conclusions depending on KPC risk thresholds.[41,43,44]

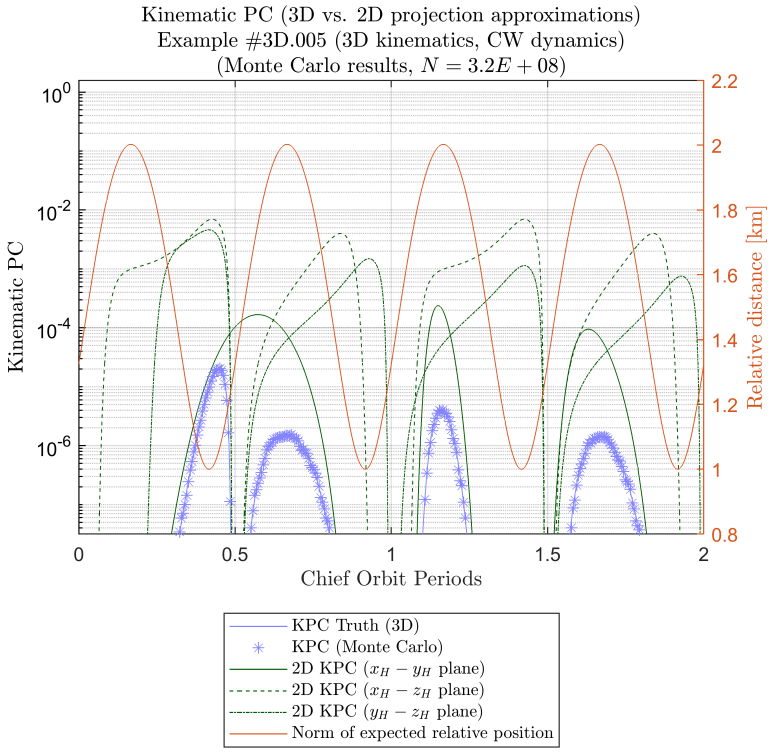

Figure 5: True KPC, projection KPCs and Monte Carlo KPC, with CW dynamics, closed orbit, normally distributed prior, Example 3D.005 (projection KPCs are normal to coordinate planes).

Motivating distance measures for correlation with true KPC

The notion of "consistency" of collision risk assessments from dissimilar collision risk indicators requires exploring the correlation between such indicators. Specifically, with the collision risk indicators considered in this work, consistency in collision risk assessments would ideally entail that local extrema of true KPC and local extrema of miss distance be anticorrelated. In other words, with consistent collision risk indicators, the true KPC waveform would ideally indicate greatest collision risk while the miss distance waveform indicates closest approach between agents in proximity. Conversely, with consistent collision risk indicators, true KPC waveform would indicate lowest collision risk while the miss distance waveform indicates furthest approach between agents.

However, as shown by the example in Figures 4 and 5, the condition of collision risk indicator consistency is not generally met when comparing the norm of expected relative position and true KPC waveforms. In this case, over a two-orbit horizon, these waveforms are mostly positively correlated. That is, primarily, true KPC indicates lowest collision risk when the norm of expected relative position indicates closest approach, and true KPC indicates highest collision risk when the norm of expected relative position indicates furthest approach. Evidently, these insights are inconsistent (as understood in this work), and using one collision risk indicator over another would lead to diametrically opposite conclusions. Even though this inconsistent indicator waveform behavior does not always occur, it is common in many of the cases considered.

Thus, the norm of expected relative position is not a miss distance waveform that can be reliably used as a qualitative substitute for (or predictor of) true KPC extrema. This finding prompts the search for other statistics of the relative position distribution that can be interpreted as miss distance and that, together with true KPC, produce consistent collision risk assessments. It is hypothesized that such a "miss distance"-like measure can be found through one of the following methodologies:

1. Methodology 1: minimum distance to a "geometric" 3-σ contour.

- This is the minimum distance to the covariance contour of the fitted relative position pdf (i.e. the relative position pdf obtained from the sample mean and covariance) at a Mahalanobis distance (MHD) of 3 away from the mean.[45]
- In this work, the prior relative state statistics are normally distributed, and since CW dynamics are linear, the distribution retains normality over time. Since the relative position pdf is three-dimensional, 97.07% of cases are within $\text{MHD} = 3$ from the mean of the pdf.

2. Methodology 2: minimum distance to an "equivalent" 3-σ contour.
   - This is the minimum distance to the covariance contour of the fitted relative position pdf at a Mahalanobis distance (MHD) so that 99.73% cases are within the corresponding MHD. In this case, $\text{MHD} = 3.7625$.
   - Probabilistically, this coincides with conventional understanding of a $3-\sigma$ event.
3. Methodology 3: 99.73% minimum distance.
   - This methodology introduces the concept of the empirical distance cumulative distribution function (cdf), which is induced through the transformation defined by the norm of relative position.[46] That is, a new cdf is created by taking the norm of the relative position of every point in the MC sample and sorting the values from such set.
   - Then, the 99.73% minimum distance is the $(100-99.73)$-percentile in the empirical distance cdf.

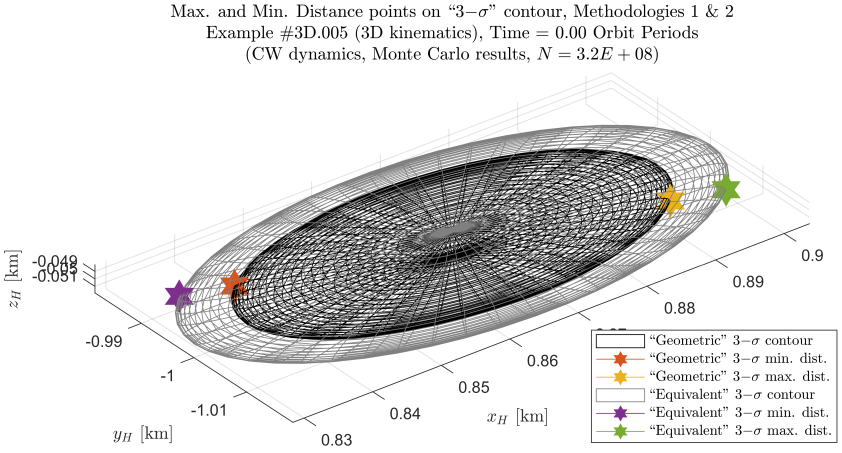

Figure 6: Fitted relative position pdf covariance contours: "geometric" 3-σ and "equivalent" 3-σ.

Miss distance measures akin to Methodologies 1 and 2 have been proposed in the literature as collision risk indicators. Wang et. al. propose a heuristic SFF COLA scheme whereby the relative position pdf is centered at the chief spacecraft instead of at the deputy spacecraft; then, an artificial potential function (APF) approach is implemented to trigger COLA actions by the deputy when its position relative to the chief crosses below a safety MHD centered at the chief's location.[33] Conceptually, the contours proposed by Wang et. al. differ from those defined by Methodologies 1 and 2 only by the specific MHD value chosen to define those contours, and by defining the center of the relative position pdf differently. The "geometric" and "equivalent" $3-\sigma$ contours, as well as points in such contours that are closest to the origin, are illustrated in Figure 6.

Methodology 3 is motivated by the existence of samples that are sufficiently large to adequately approximate the true distribution. Such a MC sample is employed in this work. Since arbitrary nonlinear transformations of each individual point in the sample can be obtained, the true miss distance of each point can be obtained as the norm of its relative position. Because of the point where the 99.73% minimum distance fits in the true distribution of miss distance (i.e. the empirical distance cdf), the measure of Methodology 3

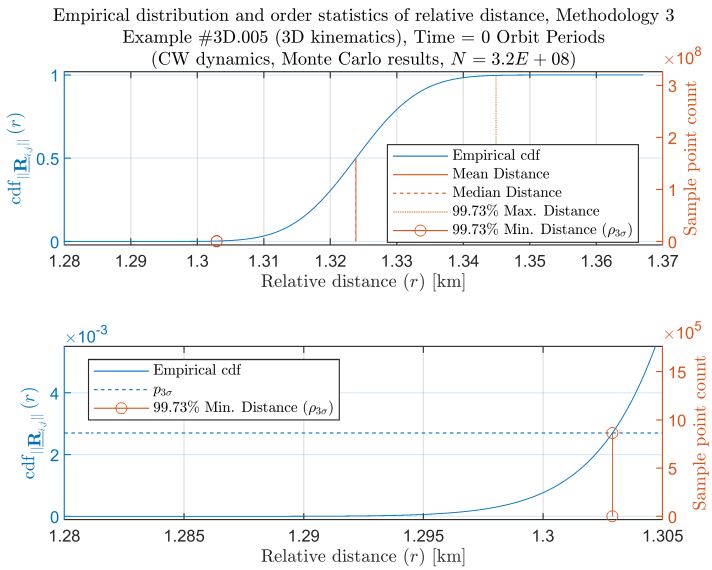

Figure 7: Empirical cumulative distribution function (cdf) of the norm of relative position (i.e. inter-agent distance): (top) complete cdf; (bottom) closeup of cdf left-tail, focusing on the 99.73% minimum distance.

can be interpreted as a "probabilistic" worst case miss distance. The 99.73% minimum distance measure is illustrated in Figure 7.

The conceptual notion of waveform correlation used in this work is formalized through the collision correlation index, $\Gamma_{i,j}$, which can be expressed in terms of a cross-correlation coefficient.[47] Specifically, $\Gamma_{i,j}$ can be expressed as the cross-correlation coefficient of $x_1(\cdot)$ and $x_2(\cdot)$ and ρ_{x_1,x_2}, i.e.

$$\Gamma_{i,j}(x_1, x_2) = \rho_{x_1,x_2} = \frac{\langle x_1(\cdot), x_2(\cdot)\rangle}{\sqrt{\mathcal{E}_{x_1}\mathcal{E}_{x_2}}} \tag{13}$$

where $x_1(\cdot)$ is the unbiased $\mathrm{KPC}_{i,j}$ signal, $x_2(\cdot)$ is the unbiased signal of a miss distance measure, and where the energy of the signal $x(\cdot)$, $\mathcal{E}_x$, is given by

$$\mathcal{E}_x \doteq \langle x(\cdot), x(\cdot)\rangle = \|x(\cdot)\|^2 \qquad \diamondsuit \tag{14}$$

The collision correlation index $\Gamma_{i,j}$ compares waveforms directly and outputs a value between -1 and 1 that indicates how correlated (or anti-correlated) the waveforms are. Thus, the notion of consistency entails that KPC and miss distance waveforms, when passed through the $\Gamma_{i,j}$ operator, should give a value as close to -1 as possible.

RESULTS AND DISCUSSION

CW simulation cases

As stated previously, dynamic scenarios in this work are assumed to follow CW dynamics. Additionally, the initial state distribution is assumed to be multivariate, non-degenerate normal. For simplicity, all cases have the same initial state covariance matrix $\Sigma_{\underline{\mathbf{X}}}(t_0)$, which is assumed to be diagonal, as given by

$$\Sigma_{\underline{\mathbf{X}}}(t_0) = \mathrm{diag}\left(\left[\sigma^2_{[x]_H}(t_0) \quad \sigma^2_{[y]_H}(t_0) \quad \sigma^2_{[z]_H}(t_0) \quad \sigma^2_{[\dot{x}]_H}(t_0) \quad \sigma^2_{[\dot{y}]_H}(t_0) \quad \sigma^2_{[\dot{z}]_H}(t_0)\right]\right) \tag{15}$$

The diagonal components of $\Sigma_{\underline{\mathbf{X}}}(t_0)$ are listed in Table 1.

Initial expected states are constrained such that propagated state expectations follow closed CW trajectories in the sense of Eqn. 8. Thus, initial state expectations $\bar{\underline{\mathbf{X}}}(t_0)$ can be (and are) prescribed in terms of the

Table 1: Initial relative state covariance parameters

Parameter at t_0	$\sigma_{[x]_H}$	$\sigma_{[y]_H}$	$\sigma_{[z]_H}$	$\sigma_{[\dot{x}]_H}$	$\sigma_{[\dot{y}]_H}$	$\sigma_{[\dot{z}]_H}$
Value	10 m	5 m	0.5 m	0.25 m/s	0.75 m/s	0.05 m/s

geometric CW parameters introduced in Eqns. 9, 10 and 11. All cases have a chief with semimajor axis $\bar{a} = 6800$ km. Then, the mean motion $\bar{n}$ can be computed in terms of Earth's standard gravitational parameter μ_E as $\bar{n} \doteq \sqrt{\mu_E/\bar{a}^3}$, where $\mu_E = 3.986004418 \times 10^5$ km^3/s^2.

The initial state expectation parameters listed in Table 2, along with the initial state covariance, are chosen so as to observe significant, nontrivial KPCs during a two-orbit propagation horizon, which is needed in order to meaningfully compare KPC signals to miss distance waveforms during such a time window. Furthermore, the focus of the Results and Discussion section is on initial state expectations where the $[x]_H$ and $[z]_H$ motion are out of phase (cases 3D.003−026); this property corresponds to a specific passive SFF COLA methodology, namely, e-i vector separation, as discussed in the Motivation section. Although all cases have expected trajectories that are collision-free, the expected trajectories in Examples 3D.003−026 provide more separation between CW chief and CW deputy during closest approach than Examples 3D.001−002.

Table 2: Initial relative state expectation parameters

Cases	Comments	$\bar{A}_0$	$\bar{B}_0$	$\bar{y}_{\text{off}}$	$\bar{\alpha}_0$	$\bar{\beta}_0 - \bar{\alpha}_0$
		[km]			[deg]	
3D.001	No $[z]_H$ motion	1	0	0	0	N/A
3D.002	With $[z]_H$ motion ($[x]_H$ and $[z]_H$ motion in phase)	1	0.1	0	0	0
3D.c ($c \in \{3, 4, \ldots, 26\}$)	With $[z]_H$ motion ($[x]_H$ and $[z]_H$ motion out of phase)	1	0.1	0	$15(c-3)$ ($\bar{\alpha}_0 \in \{0, 15, \ldots, 345\}$)	90

Finally, all cases assume joint hard-body radii of $l_{i,j} = 32$ m. This figure is based on an estimate of Hubble Space Telescope's hard body radius of $l_i = 16$ m.[48] For the purposes of this work, having such a large joint hard-body radius allows obtaining higher (and thus, more significant) KPCs. Additionally, conclusions are applicable to smaller spacecraft pairs that, by having additional buffer distance for increased safety, effectively have larger joint hard-body radii.

Validation of MC sample and projection KPC theoretical results

Figure 8 shows that the cross-correlation coefficient between sample and true KPC waveforms is approximately 1 for all dynamic cases listed in Table 2. In the limit that this cross-correlation coefficient is 1, and in the limit of continuous timesteps, this result would imply that the sample and true KPC waveforms are equal almost everywhere—to within a scaling constant. It is therefore necessary to check whether the L^2-norms of the sample and true KPC waveforms are equal (or reasonably close)— if so, then the Monte Carlo samples at hand are able to faithfully reproduce KPC waveforms, and are therefore adequate for this work.

Figure 9 shows the sample-to-true KPC waveform norm ratio for all dynamic cases listed in Table 2, which shows that the sample KPC waveform norm is within 0.84% of the true KPC waveform norm. This fact, along with the cross-correlation coefficient between these waveforms, shows that the sample KPC approximates the true KPC adequately, i.e. such waveforms coincide with low discrepancy.

Together, Figures 8 and 9 not only demonstrate the validity of the Monte Carlo samples employed in this work, but they also validate the theoretical results presented in Theorem 5 and Corollary 6 in the sense that sample KPCs coincide with true KPCs and not with projection KPCs. This notion is further reinforced with the cross-correlation coefficient between sample and projection KPCs, for both biased and unbiased waveforms, as shown in Figures and 10 and 11, respectively. These figures demonstrate that, for a wide range of initial CW conditions, there is no consistent connection between sample and projection KPCs — unlike the connection between sample and true KPCs.

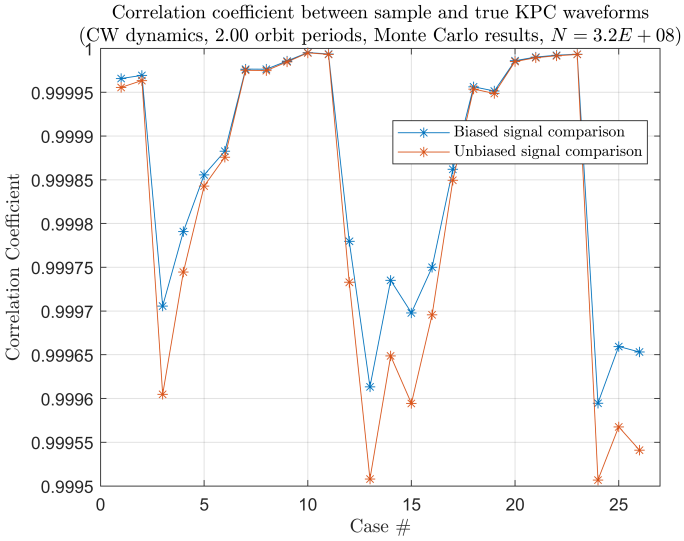

Figure 8: Cross-correlation coefficient between sample and true KPC waveforms, MC results (all cases).

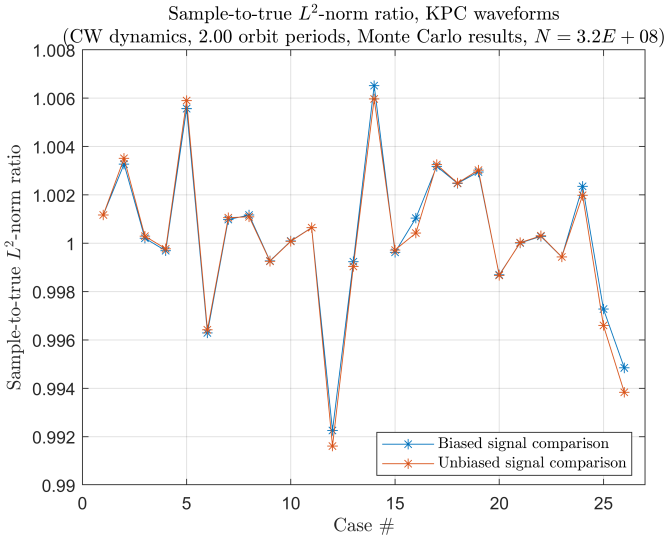

Figure 9: Sample-to-true KPC waveform L^2-norm ratios, Monte Carlo results (all cases).

Out of all dynamic cases and projections considered, there is only near agreement (to within a constant) between the sample and $[x]_H, [y]_H$-projection KPC waveforms in Case 3D.001, i.e. with no $[z]_H$ motion. However, there are two issues with the adequacy of this projection approximation. The first issue is that, as seen in Fig. 12, the $[x]_H, [y]_H$-projection KPC overestimates the sample (and true) KPC — by a factor of 2.61. This is significant because there is no projected motion that resembles the true motion as accurately as the $[x]_H, [y]_H$-projection when there is no $[z]_H$ motion. In this scenario, the expected relative trajectories are identical, and the origin of the respective collision regions is the same; the only distinction is that integrals for this projection KPC are taken over a 2D disk (as is the case for any projection KPC), whereas integrals for the sample KPC are taken over a 3D ball, as illustrated in Fig. 2. Since no other CW projection has relative motion that approximates the true relative motion better, it follows that every other CW projection case also fails to have projection KPCs that satisfactorily approximate the true KPC. The second issue is that, as discussed in the Motivation section, passive SFF COLA schemes that implement e-i vector separation are popular in applications; these schemes roughly correspond to $[x]_H$ and $[z]_H$ motion being out of phase, which implies nontrivial $[z]_H$ motion. Thus, even if $[x]_H, [y]_H$-projection KPCs were adequate for the case of no

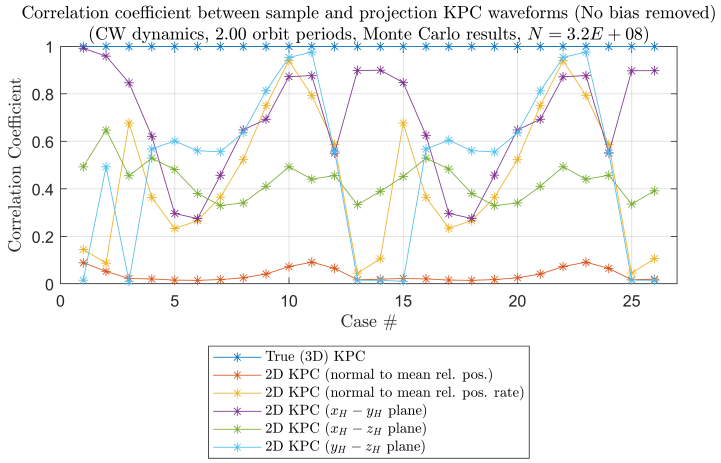

Figure 10: Cross-correlation coefficient between sample and projection KPC waveforms, Monte Carlo results (all cases, biased waveforms).

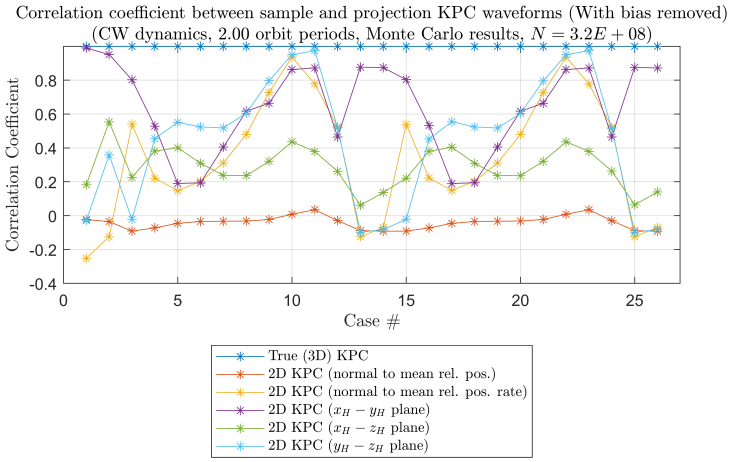

Figure 11: Cross-correlation coefficient between sample and true KPC waveforms, Monte Carlo results (all cases, unbiased waveforms).

$[z]_H$ motion, $[x]_H, [y]_H$-projection KPCs would not be adequate when e-i vector separation is implemented. Therefore, Figures 8-12 demonstrate that there are no general CW dynamics cases where any projection KPC waveform adequately approximates a true KPC waveform.

Correlating miss distance and true KPC

In this work, true KPC and "miss distance"-like measures represented by Methodologies 1, 2 and 3 are compared in order to examine the consistency of collision risk assessments obtained by these comparisons. For the case of no $[z]_H$ motion (see Figure 13) and for the case of $[x]_H$ and $[z]_H$ motion in phase (see Figure 14), such comparisons are illustrated through the true KPC and miss distance waveforms themselves; for the case of $[x]_H$ and $[z]_H$ motion out of phase, the comparison is made through the collision correlation index.

It is found that there is no general correlation between the unbiased waveforms of the KPC and the norm of expected relative position, since local extrema of the former and the latter are positively correlated as frequently as they are negatively correlated, and often, there is no correlation between the two waveforms. In

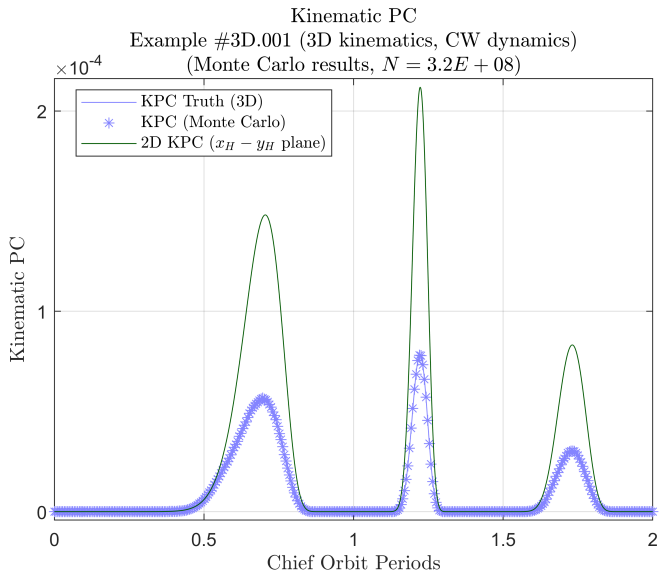

Figure 12: Sample, true and $[x]_H$-$[y]_H$ projection KPC waveforms, Example 3D.001.

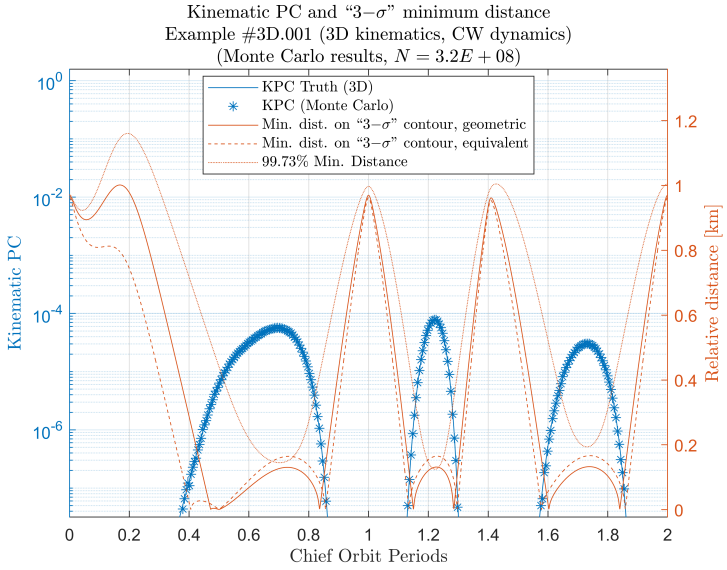

Figure 13: Comparison of KPC and "miss distance"-like waveforms, Methodologies 1, 2 and 3, Example 3D.001 (no $[z]_H$ motion).

contrast, Methodologies 1–3, together with the true KPC, exhibit either negative or null collision correlation indices over several cases of out-of-phase radial/cross-track motion, and this is observed more strongly for $\rho_{3\sigma}$ than for Methodologies 1 and 2. Thus, Methodology 3, together with the true KPC, produces the most consistent collision risk assessment under the collision correlation index criterion. Hence, Figures 13-15 indicate that the degree of correspondence between KPC and $\rho_{3\sigma}$ changes is greater than between KPC and Methodology 1 or 2 changes, which indicates that the KPC and $\rho_{3\sigma}$ are more qualitatively interchangeable than the KPC and Methodology 1 or 2. Thus, of all the statistical descriptions of agent separation considered, $\rho_{3\sigma}$ is the most intuitively related to the KPC as per the discussion in the Theory section.

Although the distance measure of Methodology 3 (together with the true KPC) produces correlation indices that are consistently closer to -1 than any other distance measure, this relationship is distinct from—and does

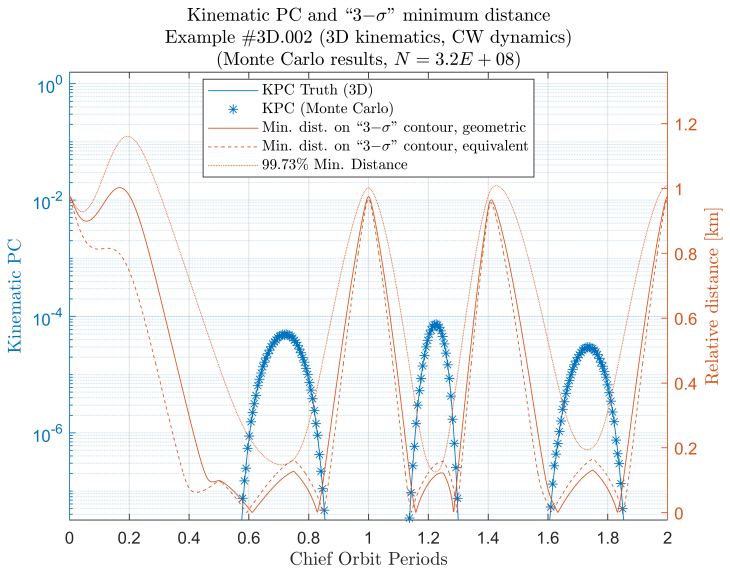

Figure 14: Comparison of KPC and "miss distance"-like waveforms, Methodologies 1, 2 and 3, Example 3D.002 ($[x]_H$ and $[z]_H$ motion in phase).

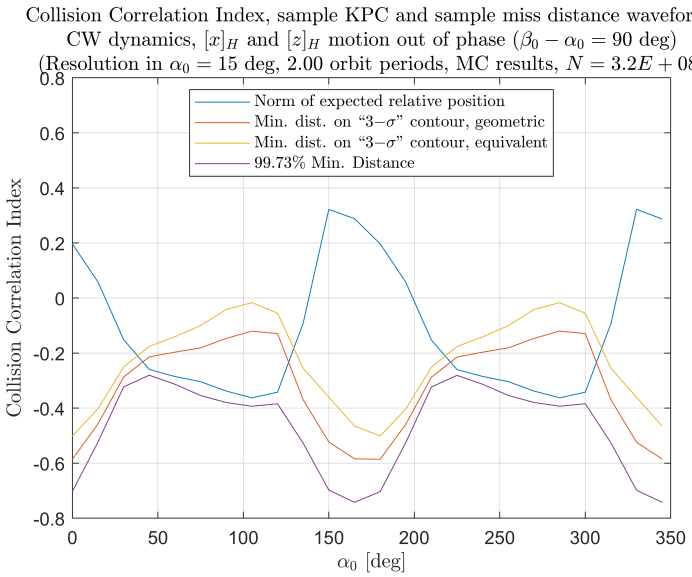

Figure 15: Collision correlation index between true KPC and "miss distance"-like waveforms, Methodologies 1, 2 and 3, and norm of expected relative position ($[x]_H$ and $[z]_H$ motion out of phase).

not closely approximate—linear dependence. In fact, the anti-correlation between the unbiased Methodology 3 distance measure and the unbiased true KPC waveform is much weaker than the correlation between certain projection KPCs and true KPCs. Yet, the conclusion is that projection KPCs are inadequate for approximating true KPCs, while Methodology 3 is considered to be an adequate surrogate for the true KPC. The reason for this interpretation is that, not only are distance measures and true KPCs conceptually and physically distinct, but employing one criterion over the other as an indicator of collision risk already leads to distinct active SFF COLA philosophies, as discussed in the Motivation section. Thus, the significant aspect of the relationship between Methodology 3 and true KPCs is that, despite their conceptual distinction, they are still related to each other in a way that is consistent with intuition, and even though their anti-correlation is not as strong as it could be, their anti-correlation is still stronger for Methodology 3 than for other distance measures over a

wide range of CW dynamic cases. Therefore, it is adequate to state that Methodology 3 (together with KPC) is more likely to produce consistent collision risk assessments than other distance measures. Moreover, it is concluded that Methodology 3 is a better predictor of true KPC (and vice versa) than other distance measures considered, which is a helpful heuristic in applications where only one method of active SFF COLA is implemented.

Comparing Methodology 3 and window probability of collision

Since the true KPC and the separation measure of Methodology 3 (i.e. 99.73% min distance) produce consistent collision risk assessments, it is helpful to examine how these two collision risk indicators relate to the window probability of collision (WPC), where the WPC is the probability of collision at any time within a given time window.[49] When combining these three indicators, it is found that they are consistent and complementary, as they all indicate consistent aspects of the same collision assessment. That is, at the same time, the true KPC has local maxima, the WPC indicates increased risk of collision, and 99.73% min distance indicates "closest approach" between the chief and deputy spacecraft, as depicted in Figure 16.

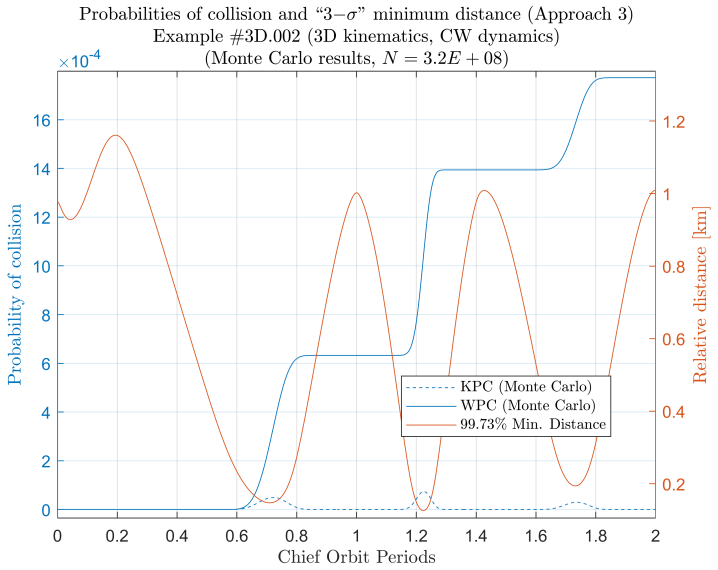

Figure 16: Comparison of KPC, WPC and 99.73% minimum distance waveforms.

The consistency of the true KPC, WPC and 99.73% min distance waveforms is a significant result for the SFF COLA community. By employing these collision risk indicators in unison, it is possible to obtain consistent collision risk assessments, which is valuable in the distinct yet complementary goals of SFF mission safety and operational performance. Additionally, by unifying the two main collision risk indicators found in the literature, a step toward bridging their corresponding SFF COLA philosophies into an unified framework is achieved.

CONCLUSION

In this work, several paradigms are addressed regarding collision risk assessment practices in the context of spacecraft formation flying (SFF) collision avoidance (COLA). The first area of contribution pertains to the true and projection kinematic probabilities of collision (KPCs), which are defined using topological notions and employing the hard body radius assumption. It is proven (in Theorem 5) that for continuous relative position probability density functions (pdfs), any choice of projection KPC always overestimates the true KPC. This result is validated through Monte Carlo simulation in an environment subject to CW dynamics for a wide range of initial conditions. This result implies that using projection KPCs instead of true KPCs in collision risk assessment results in probabilistic false positives in the detection of high collision risk events, which is detrimental to agents in spacecraft formations with limited, non-renewable onboard

propellant. Therefore, it is concluded that employing projection KPCs for collision risk assessment in the context of SFF COLA is an inadequate practice.

The second area of contribution pertains to the "consistency" of collision risk assessments based on separation measures and true KPCs. This notion explores the question of whether or not separation measures and true KPC waveforms are related in accordance with intuition, namely, where minimum separation is correlated with highest collision probability, and where maximum separation is correlated with lowest collision probability. The notion of "consistency" is quantified through the collision correlation index introduced in the Theory section. On the one hand, it is found that a certain separation measure (namely, the $100(1-0.9973\ldots)$-percentile in the empirical distance distribution, or $\rho_{3\sigma}$), together with true KPC, produces consistent collision risk assessments over a wide range of CW initial conditions in the sense that the collision correlation index is always negative, although not to the extent of indicating linear dependence. On the other hand, it is found that the norm of expected relative position, together with true KPC does not produce consistent assessments, while two separation measures (distance from the origin to a "geometric" $3-\sigma$ contour, and distance from the origin to an "equivalent" $3-\sigma$ contour) produce assessments that, while consistent, exhibit a lesser degree of correspondence with the true KPC than the $\rho_{3\sigma}$ indicator. These results give insight into the tradeoffs of choosing one of the two main philosophies of high collision risk event detection (miss distance-based and KPC-based detection) over the other.

The contributions made by this work prompt new directions for future research in SFF collision risk assessment. First, given that waveforms of the separation measure defined by Methodology 3 (i.e. the $100(1-0.9973\ldots)$-percentile in the empirical distance distribution) are, in some sense, surrogates for true KPC waveforms, it would be beneficial to develop ways to compute such separation waveforms or approximate them numerically; doing so would help avoid estimating them through a computationally costly sampling method. Thus, the distance measure of Methodology 3 could be employed in real-time applications where collision risk assessments are based on separation measures. Second, it would be helpful to examine if it is possible to translate safety requirements defined in terms of true KPCs into requirements expressed in terms of separation measures. This would enable approximate equivalency between collision risk assessment philosophies. Third, collision safety requirements in SFF applications could be stated in a way that defines high-risk event criteria in terms of both true KPCs and some of the separation measures defined in this work. This would allow for the creation of more nuanced safety criteria than is possible when only one high-risk event detection philosophy is employed. If this avenue of research is pursued, it would also be important to see how COLA maneuver planning and execution would be affected by these changes in high-risk event detection and constraint satisfaction criteria. Fourth, given how both true KPCs and separation measures are based on underlying relative state statistics, it would be beneficial to explore how relative state knowledge accuracy and propagation horizons affect not only true KPCs and separation measures, but also their connection. This would be important in establishing requirements for onboard measurement and filtering update rates and necessary accuracy. Fifth, it would be beneficial to examine whether the conclusions of this work hold in relative orbital dynamic environments that can be better described as distinct from CW dynamics, e.g. by accounting for dynamic perturbations (such as higher order gravity terms, drag etc.) or by using different relative state representations (such as curvilinear coordinates or relative orbit elements).

REFERENCES

[1] D. P. Scharf, F. Y. Hadaegh, and S. R. Ploen, "A survey of spacecraft formation flying guidance and control (part I): guidance," *Proceedings of the 2003 American Control Conference*, Vol. 2, Denver, CO, IEEE, Jun. 2003, pp. 1733–1739, 10.1109/ACC.2003.1239845.

[2] K. Alfriend, S. R. Vadali, P. Gurfil, J. How, and L. Breger, *Spacecraft Formation Flying: Dynamics, Control and Navigation*, ch. 1, 14, pp. 1–11, 329–330. Elsevier Astrodynamics Series, Oxford, UK: Butterworth–Heinemann (Elsevier Science), 2010.

[3] J. R. Wertz, "Mission Concept Definition and Exploration," *Space Mission Engineering: The New SMAD* (J. R. Wertz, D. F. Everett, and J. J. Puschell, eds.), Space Technology Library, ch. 4, pp. 61–82, Hawthorne, CA: Microcosm Press, 2011.

[4] S. J. Chung, S. Bandyopadhyay, R. Foust, G. P. Subramanian, and F. Hadaegh, "Review of Formation Flying and Constellation Missions Using Nanosatellites," *Journal of Spacecraft and Rockets*, Vol. 53, No. 3, 2016, pp. 567–578, 10.2514/1.A33291.

[5] H. Schaub and J. L. Junkins, "Spacecraft Formation Flying," *Analytical Mechanics of Space Systems*, ch. 14, pp. 593–673, Reston, VA: AIAA Education Series, 2nd ed., 2009, 10.2514/4.105210.

[6] B. Tapley, J. Ries, S. Bettadpur, D. Chambers, M. Cheng, F. Condi, B. Gunter, Z. Kang, P. Nagel, R. Pastor, T. Pekker, S. Poole, and F. Wang, "GGM02 – An improved Earth gravity field model from GRACE," *Journal of Geodesy*, Vol. 79, Nov. 2005, pp. 467–478, 10.1007/s00190-005-0480-z.

[7] A. K. Sugihara El Maghraby, A. Grubisic, C. Colombo, and A. Tatnall, "A novel approach to microwave interferometric radiometry in the geostationary orbit using formation flight," *67th International Astronautical Congress of the International Astronautical Federation*, Guadalajara, Mexico, Sep. 2016, pp. 1–14.

[8] A. W. Koenig, B. Macintosh, and S. D'Amico, "Formation Design of Distributed Telescopes in Earth Orbit for Astrophysics Applications," *Journal of Spacecraft and Rockets*, Vol. 56, No. 5, 2019, pp. 1462–1477, 10.2514/1.A34420.

[9] G. Wang and W. T. Ni, "Numerical simulation of time delay interferometry for eLISA/NGO," *Classical and Quantum Gravity*, Vol. 30, Feb. 2013, pp. 1–19, 10.1088/0264-9381/30/6/065011.

[10] G. W. Hill, "Researches in the Lunar Theory," *American Journal of Mathematics*, Vol. 1, No. 1, 1878, pp. 5–26, 10.2307/2369430.

[11] W. H. Clohessy and R. S. Wiltshire, "Terminal guidance system for satellite rendezvous," *Journal of Aerospace Sciences*, Vol. 27, No. 9, 1960, pp. 653–658, 10.2514/8.8704.

[12] B. Naasz, "Safety Ellipse Motion with Coarse Sun Angle Optimization," *595 Flight Mechanics Symposium*, Greenbelt, MD, NASA Goddard Space Flight Center, Oct. 2005, pp. 1–13.

[13] S. D'Amico and O. Montenbruck, "Proximity Operations of Formation-Flying Spacecraft Using an Eccentricity/Inclination Vector Separation," *Journal of Guidance, Control, and Dynamics*, Vol. 29, No. 3, 2006, pp. 554–563, 10.2514/1.15114.

[14] O. Montenbruck, R. Kahle, S. D'Amico, and J.-S. Ardaens, "Navigation and control of the TanDEM-X formation," *The Journal of the Astronautical Sciences*, Vol. 56, Sep. 2008, pp. 341–357, 10.1007/BF03256557.

[15] S. D'Amico, J.-S. Ardaens, and R. Larsson, "Spaceborne Autonomous Formation-Flying Experiment on the PRISMA Mission," *Journal of Guidance, Control, and Dynamics*, Vol. 35, No. 3, 2012, pp. 834–850, 10.2514/1.55638.

[16] P. Liu, X. Chen, and Y. Zhao, "Safe deployment of cluster-flying nano-satellites using relative E/I vector separation," *Advances in Space Research*, Vol. 64, No. 4, 2019, pp. 964–981, 10.1016/j.asr.2019.05.036.

[17] P. Palmer and M. Halsall, "Designing Natural Formations of Low-Earth-Orbiting Satellites," *Journal of Guidance, Control, and Dynamics*, Vol. 32, No. 3, 2009, pp. 860–868, 10.2514/1.39631.

[18] D. Morgan, S.-J. Chung, L. Blackmore, B. Acikmese, D. Bayard, and F. Y. Hadaegh, "Swarm-Keeping Strategies for Spacecraft Under J2 and Atmospheric Drag Perturbations," *Journal of Guidance, Control, and Dynamics*, Vol. 35, No. 5, 2012, pp. 1492–1506, 10.2514/1.55705.

[19] R. Opromolla, G. Fasano, G. Rufino, and M. Grassi, "Design of relative trajectories for in orbit proximity operations," *Acta Astronautica*, Vol. 145, Apr. 2018, pp. 342–356, 10.1016/j.actaastro.2018.01.062.

[20] A. Richards, T. Schouwenaars, J. P. How, and E. Feron, "Spacecraft Trajectory Planning with Avoidance Constraints Using Mixed-Integer Linear Programming," *Journal of Guidance, Control, and Dynamics*, Vol. 25, No. 4, 2002, pp. 755–764, 10.2514/2.4943.

[21] Y. Kim, M. Mesbahi, and F. Y. Hadaegh, "Multiple-spacecraft reconfiguration through collision avoidance, bouncing, and stalemate," *Journal of Optimization Theory and Applications*, Vol. 122, No. 2, 2004, pp. 323–343, 10.1023/B:JOTA.0000042524.57088.8b.

[22] J. B. Mueller and R. Larsson, "Collision avoidance maneuver planning with robust optimization," *7th International ESA Conference on Guidance, Navigation & Control Systems*, Tralee, Ireland, European Space Agency, Jun. 2008, pp. 1–16.

[23] J. Mueller, "Onboard Planning of Collision Avoidance Maneuvers Using Robust Optimization," *AIAA Infotech@Aerospace Conference*, Seattle, WA, AIAA, Apr. 2009, pp. 1–17, 10.2514/6.2009-2051.

[24] H. Min, Z. Guoqiang, and S. Junling, "Collision Avoidance Control for Formation Flying Satellites," *AIAA Guidance, Navigation, and Control Conference*, Toronto, Canada, AIAA, Aug. 2010, pp. 1–9, 10.2514/6.2010-7714.

[25] Z. Guoqiang, H. Min, and S. Junling, "Collision monitoring and optimal collision avoidance manoeuvre for formation flying satellites," *Aircraft Engineering and Aerospace Technology*, Vol. 84, Jan. 2012, pp. 413–422, 10.1108/00022661211272963.

[26] J. B. Mueller, P. R. Griesemer, and S. J. Thomas, "Avoidance Maneuver Planning Incorporating Station-Keeping Constraints and Automatic Relaxation," *Journal of Aerospace Information Systems*, Vol. 10, No. 6, 2013, pp. 306–322, 10.2514/1.54971.

[27] X. Chu, J. Zhang, S. Lu, Y. Zhang, and Y. Sun, "Optimised collision avoidance for an ultra-close rendezvous with a failed satellite based on the Gauss pseudospectral method," *Acta Astronautica*, Vol. 128, Nov.-Dec. 2016, pp. 363–376, 10.1016/j.actaastro.2016.07.011.

[28] Z. Xu, X. Chen, Y. Huang, Y. Bai, and Q. Chen, "Collision prediction and avoidance for satellite ultra-close relative motion with zonotope-based reachable sets," *Proceedings of the Institution of Mechanical Engineers, Part G: Journal of Aerospace Engineering*, Vol. 233, No. 11, 2019, pp. 3920–3937, 10.1177/0954410018810255.

[29] R. Bevilacqua, T. Lehmann, and M. Romano, "Development and experimentation of LQR/APF guidance and control for autonomous proximity maneuvers of multiple spacecraft," *Acta Astronautica*, Vol. 68, No. 7, 2011, pp. 1260–1275, 10.1016/j.actaastro.2010.08.012.

[30] I. Okoloko, "Path planning for multiple spacecraft using consensus with LMI avoidance constraints," *2012 IEEE Aerospace Conference*, Mar. 2012, pp. 1–8, 10.1109/AERO.2012.6187118.

[31] S. Nag and L. Summerer, "Behaviour based, autonomous and distributed scatter manoeuvres for satellite swarms," *Acta Astronautica*, Vol. 82, No. 1, 2013, pp. 95–109, 10.1016/j.actaastro.2012.04.030.

[32] X. Lin, X. Shi, and S. Li, "Optimal cooperative control for formation flying spacecraft with collision avoidance," *Science Progress*, Vol. 103, No. 1, 2020, pp. 1–19, 10.1177/0036850419884432.

[33] Y. Wang, Y. Bai, J. Xing, G. Radice, Q. Ni, and X. Chen, "Equal-collision-probability-curve method for safe spacecraft close-range proximity maneuvers," *Advances in Space Research*, Vol. 62, No. 9, 2018, pp. 2599–2619, 10.1016/j.asr.2018.07.007.

[34] Y. Wang, X. Chen, D. Ran, Y. Zhao, Y. Chen, and Y. Bai, "Spacecraft formation reconfiguration with multi-obstacle avoidance under navigation and control uncertainties using adaptive artificial potential function method," *Astrodynamics*, Vol. 4, Mar. 2020, pp. 41–56, 10.1007/s42064-019-0049-x.

[35] G. L. Slater, S. M. Byram, and T. W. Williams, "Collision Avoidance for Satellites in Formation Flight," *Journal of Guidance, Control, and Dynamics*, Vol. 29, No. 5, 2006, pp. 1140–1146, 10.2514/1.16812.

[36] R. Serra, D. Arzelier, M. Joldes, and A. Rondepierre, "Probabilistic Collision Avoidance for Long-term Space Encounters via Risk Selection," *Advances in Aerospace Guidance, Navigation and Control: Third CEAS Specialist Conference on Guidance, Navigation and Control* (J. Bordeneuve-Guibé, A. Drouin, and C. Roos, eds.), Toulouse, France, Springer International Publishing, Apr. 2015, pp. 679–698, 10.1007/978-3-319-17518-8_39.

[37] J.-B. Caillau, M. Cerf, A. Sassi, E. Trélat, and H. Zidani, "Solving chance constrained optimal control problems in aerospace via kernel density estimation," *Optimal Control Applications and Methods*, Vol. 39, No. 5, 2018, pp. 1833–1858, 10.1002/oca.2445.

[38] C. Heil, *Introduction to Real Analysis*, ch. 1–2, 7–8, pp. 15–86, 253–326. Graduate Texts in Mathematics, Cham: Springer International Publishing, 2019, 10.1007/978-3-030-26903-6.

[39] M. R. Akella and K. T. Alfriend, "Probability of Collision Between Space Objects," *Journal of Guidance, Control, and Dynamics*, Vol. 23, No. 5, 2000, pp. 769–772, 10.2514/2.4611.

[40] R. P. Patera, "General Method for Calculating Satellite Collision Probability," *Journal of Guidance, Control, and Dynamics*, Vol. 24, No. 4, 2001, pp. 716–722, 10.2514/2.4771.

[41] L. K. Newman, R. C. Frigm, M. G. Duncan, and M. D. Hejduk, "Evolution and Implementation of the NASA Robotic Conjunction Assessment Risk Analysis Concept of Operations," *2014 Advanced Maui Optical and Space Surveillance Technologies Conference Proceedings*, Maui, HI, Sep. 2014, pp. 1–14.

[42] D. P. Kroese, T. Taimre, and Z. I. Botev, "Probability Distributions," *Handbook of Monte Carlo Methods*, ch. 4, pp. 85–151, John Wiley & Sons, Ltd., 2011, 10.1002/9781118014967.ch4.

[43] M. D. Hejduk and L. C. Johnson, "Approaches to Evaluating Probability of Collision Uncertainty," *26th AAS/AIAA Space Flight Mechanics Meeting*, AAS 16-241, Napa, CA, AAS/AIAA, Feb. 2016, pp. 1–15.

[44] M. D. Hejduk, "CARA Risk Assessment Thresholds," *2016 International Conjunction Assessment Technical Advisory Council Meeting*, GSFC-E-DAA-TN31654, Paris, France, Centre National d'Etudes Spatiales, May 2016, pp. 1–26.

[45] P. Bhattacharya and P. Burman, "12 - Multivariate Analysis," *Theory and Methods of Statistics*, pp. 383–429, Academic Press, 2016, 10.1016/B978-0-12-802440-9.00012-6.

[46] H. Schwarzlander, "Part 4: Transformations and Multiple Random Variables," *Probability Concepts and Theory for Engineers*, ch. 4, pp. 227–304, John Wiley & Sons, Ltd., 2011, 10.1002/9781119990895.ch4.

[47] J. Proakis and M. Salehi, "Deterministic and Random Signal Analysis," *Digital Communications*, ch. 2, pp. 17–94, New York, NY: McGraw-Hill, 5th ed., 2008.

[48] Lockheed Martin, "Introduction," *Hubble Space Telescope Servicing Mission 3B: Media Reference Guide*, NP-2001-12-412-GSFC, NASA Goddard Space Flight Center, 2001, pp. 1–7.

[49] R. C. Frigm, M. D. Hejduk, L. C. Johnson, and D. Plakalovic, "Total Probability of Collision as a Metric for Finite Conjunction Assessment and Collision Risk Management," *2015 Advanced Maui Optical and Space Surveillance Technologies Conference Proceedings*, Maui, HI, Jan. 2015, pp. 1–14.